

Synchronized Northern Hemisphere climate change and solar magnetic cycles during the Maunder Minimum

Yasuhiko T. Yamaguchi^{a,b,c}, Yusuke Yokoyama^{a,b,c,1}, Hiroko Miyahara^d, Kenjiro Sho^e, and Takeshi Nakatsuka^{f,g}

^aAtmosphere and Ocean Research Institute, The University of Tokyo, 5-1-5 Kashiwanoha, Kashiwa 275-8564, Japan; ^bDepartment of Earth and Planetary Science, The University of Tokyo, 7-3-1 Hongo, Bunkyo-ku, Tokyo 113-0033, Japan; ^cInstitute of Biogeosciences, Japan Agency for Marine-Earth Science and Technology, 2-15, Natsushima-cho, Yokosuka 237-0061, Japan; ^dInstitute for Cosmic Ray Research, The University of Tokyo, 5-1-5 Kashiwanoha, Kashiwa 277-8582, Japan; ^eDepartment of Civil Engineering and Systems Management, Nagoya Institute of Technology, Gokiso-cho, Showa-ku, Nagoya 466-8555, Japan; ^fInstitute of Low Temperature Science, Hokkaido University, N19 W8, Kita-ku, Sapporo 060-0819, Japan; and ^gGraduate School of Environmental Studies, Nagoya University, Furo-cho, Chikusa-ku, Nagoya 464-8601, Japan

Edited by Konrad A. Hughen, Woods Hole Oceanographic Institute, Woods Hole, MA, and accepted by the Editorial Board October 8, 2010 (received for review January 6, 2010)

The Maunder Minimum (A.D. 1645–1715) is a useful period to investigate possible sun–climate linkages as sunspots became exceedingly rare and the characteristics of solar cycles were different from those of today. Here, we report annual variations in the oxygen isotopic composition ($\delta^{18}\text{O}$) of tree-ring cellulose in central Japan during the Maunder Minimum. We were able to explore possible sun–climate connections through high-temporal resolution solar activity (radiocarbon contents; $\Delta^{14}\text{C}$) and climate ($\delta^{18}\text{O}$) isotope records derived from annual tree rings. The tree-ring $\delta^{18}\text{O}$ record in Japan shows distinct negative $\delta^{18}\text{O}$ spikes (wetter rainy seasons) coinciding with rapid cooling in Greenland and with decreases in Northern Hemisphere mean temperature at around minima of decadal solar cycles. We have determined that the climate signals in all three records strongly correlate with changes in the polarity of solar dipole magnetic field, suggesting a causal link to galactic cosmic rays (GCRs). These findings are further supported by a comparison between the interannual patterns of tree-ring $\delta^{18}\text{O}$ record and the GCR flux reconstructed by an ice-core ^{10}Be record. Therefore, the variation of GCR flux associated with the multidecadal cycles of solar magnetic field seem to be causally related to the significant and widespread climate changes at least during the Maunder Minimum.

solar forcing of climate | little ice age | paleoclimate reconstruction | grand solar minimum | tree-ring isotope climatology

There is a long-standing controversy on whether solar activity can significantly influence climate, and how this might occur (1). Although the most straightforward mechanism of the sun–climate connection is the direct heating of the earth by solar radiation [total solar irradiance (TSI)], it is unlikely that the entire solar influence on climate can be attributed simply to variations in the TSI (2–4). Other major possible mechanisms include solar ultraviolet (UV) radiation that promotes chemical reactions in the upper atmosphere (5–8) and galactic cosmic rays (GCRs). The latter are modulated by solar and terrestrial magnetic activity, and may enhance cloud formation (9–13). However, it is difficult to evaluate the exact role of each solar parameter in climate change, because instrumentally measured solar-related parameters such as TSI, UV, and GCR fluxes are more or less synchronized and only extend back for several decades.

Many studies have claimed that past climate records show a correlation with solar activity [e.g., proxy records including ice rafted debris in marine sediments (14), composition of lake sediments (15–17), oxygen isotopic composition ($\delta^{18}\text{O}$) in stalagmites (18–21), $\delta^{18}\text{O}$ in corals (22), $\delta^{18}\text{O}$ in ice cores (23) and variations in tree-ring widths (24)]. The main evidence derives from correlated periodicities in climate and solar activities (e.g., 11, 22, 88, or 205 years). However, in climate records, it is difficult to

discriminate between externally caused variations and internally caused “solar-like periodicities.” Moreover, there is ambiguity and possibly spurious coincidences between climate cycles and solar activity; mainly because the reconstructed climate records dated with radio-nuclides include significant dating errors, whereas solar activity determined from radiocarbon contents ($\Delta^{14}\text{C}$) in tree rings is based on dendro-chronology with smaller dating uncertainties (25).

During the Maunder Minimum (A.D. 1645–1715) (26) solar activity and GCR flux variations reconstructed by tree-ring $\Delta^{14}\text{C}$ were distinct. Firstly, the wavelet analysis of tree-ring $\Delta^{14}\text{C}$ showed that the length of solar cycles during the Maunder Minimum were a few years longer (14 and 28 years) than those of today (11 and 22 years) (27). Secondly, variations in the GCR flux are believed to have been different from that of today because of the different mode of solar magnetic cycles (28, 29). Based on these features, the effects of solar activity and GCRs on climate can be distinguished from internal climate variations. Recently, we have found that the variations in Greenland temperatures reconstructed from $\delta^{18}\text{O}$ of 7 ice cores (30) coincide with the “22 year” (actually 28 year) variations in GCRs during the Maunder Minimum, suggesting a possible influence of GCRs on the decadal to multidecadal climate changes (29). However, the spatial resolution of the climate records was not well characterized. Moreover, ice-core records possibly have dating errors of a few years, which make it difficult to discuss the sun–climate connection precisely.

We, therefore, investigated the annual $\delta^{18}\text{O}$ variations in tree-ring cellulose from central Japan during the Maunder Minimum. This enables a direct comparison with tree-ring $\Delta^{14}\text{C}$ records and an understanding of spatial distribution of climate variations. To our knowledge, this is the first paper to compare tree-ring cellulose $\delta^{18}\text{O}$ directly with tree-ring $\Delta^{14}\text{C}$. Tree-ring $\delta^{18}\text{O}$ is correlated negatively with relative humidity and positively with $\delta^{18}\text{O}$ in precipitation (31). Because $\delta^{18}\text{O}$ in precipitation is negatively correlated with the amount of precipitation in monsoon areas (32), the tree-ring $\delta^{18}\text{O}$ can be a reliable proxy for past relative humidity and/or amount of precipitation in Japan (33–35). In humid and temperate regions, variations in tree-ring width and its carbon isotopic composition ($\delta^{13}\text{C}$) often show large discre-

Author contributions: Y.Y. and H.M. designed research; Y.T.Y., K.S., and T.N. performed research; T.N. contributed new reagents/analytic tools; Y.T.Y., Y.Y., and H.M. analyzed data; and Y.T.Y., Y.Y., and H.M. wrote the paper.

The authors declare no conflict of interest.

This article is a PNAS Direct Submission. K.A.H. is a guest editor invited by the Editorial Board.

¹To whom correspondence should be addressed. E-mail: yokoyama@aori.u-tokyo.ac.jp.

This article contains supporting information online at www.pnas.org/lookup/suppl/doi:10.1073/pnas.1000113107/-DCSupplemental.

pancies between different individual trees mainly due to ecological competition in forest areas of high population density. However, even in these circumstances the interannual variations in tree-ring $\delta^{18}\text{O}$ are well correlated among different trees and accurately reflect the regional hydroclimate variations (33). The annual time resolution is sufficient to investigate climate periodicities at the decadal scale and to reveal the response time of climate to changes in solar activity.

We have determined the tree-ring cellulose $\delta^{18}\text{O}$ of a Japanese cedar tree (*Cryptomeria japonica*) collected at “Nara” and a Japanese cypress tree (*Chamaecyparis obtuse*) collected at “Shiga.” The Shiga cypress served as a calibration because its growth spanned the twentieth century and a close meteorological station provided direct meteorological data extending back to A.D. 1881. The 392 year old Nara cedar grew between A.D. 1607–1998, which includes the Maunder Minimum period. During the twentieth century its $\delta^{18}\text{O}$ record has only 35 discontinuous years due to narrow tree-ring widths (see *Materials and Methods*).

Results and Discussion

Single correlation analysis was carried out at each site between the tree-ring cellulose $\delta^{18}\text{O}$ records and monthly meteorological data obtained from the closest meteorological stations for the same year. The analyses covered the average monthly temperature, monthly precipitation, and the average monthly relative humidity (Fig. 1 *A–B* and Fig. S1). The highest correlation (negative value) was found between $\delta^{18}\text{O}$ and relative humidity in June at both sites ($r = -0.695$ in Nara, $p < 0.001$; $r = -0.723$ in Shiga, $p < 0.001$; Fig. 1 *C–D*), whereas the correlations were lower for temperature ($r = 0.489$ in Nara, $r = 0.501$ in Shiga) and precipitation ($r = -0.351$ in Nara, $r = -0.345$ in Shiga). The coincidence in the correlation patterns between the two trees indicates the reliability of the tree-ring cellulose $\delta^{18}\text{O}$ records as climate proxy for central Japan. We also compared the tree-ring

cellulose $\delta^{18}\text{O}$ with relative humidity in June obtained at 96 meteorological stations across Japan (Fig. 2 *A–B*). High correlation coefficients (< -0.6 in Nara, $p < 0.001$; < -0.5 in Shiga, $p < 0.001$) were found across a wide area of central Japan. This suggests that the main controlling factor over the tree-ring cellulose $\delta^{18}\text{O}$ in central Japan is the East Asian summer monsoon (EASM), as EASM strongly affects the rainy season (June–July) in central Japan by moisture transport via the characteristic stationary front (the Baiu front).

The tree-ring cellulose $\delta^{18}\text{O}$ data from the Nara cedar during A.D. 1612–1756 are plotted in Fig. 3. The figure includes winter-temperature index in southern Greenland reconstructed from ice-core records (30), reconstructed Northern Hemisphere (NH) mean temperature from multiple proxies (36), reconstructed ^{14}C production anomaly using tree-ring $\Delta^{14}\text{C}$ (25), group sunspot numbers (37), and ^{10}Be flux from the North Greenland Ice Core Project (NGRIP) ice core in Greenland (38) during A.D. 1612–1760. Note that ^{14}C provides exact timing of solar-related GCR cycles, whereas the amplitude variation is not reliable due to the measurement errors comparable to the largely attenuated ^{14}C variation in tree rings. Based on these record, we find the following correlations between the Japanese tree ring and solar records: The large negative $\delta^{18}\text{O}$ spikes, the rapid cooling events in Greenland, and the decreases in the mean temperature in the NH records are all synchronous with the solar minima (high ^{14}C production anomaly) when solar magnetic field polarity was negative during the Maunder Minimum (blue bars and open circles) and at the solar minima with positive polarity after the Maunder Minimum (red bars and open circles).

At these solar minima with negative polarity, the GCR flux may have been particularly high due to physical mechanisms described below. The trajectory of GCRs (mainly protons) in the heliosphere is strongly dependent on the polarity of solar dipole magnetic field because of the drift effect of GCRs along the wavy

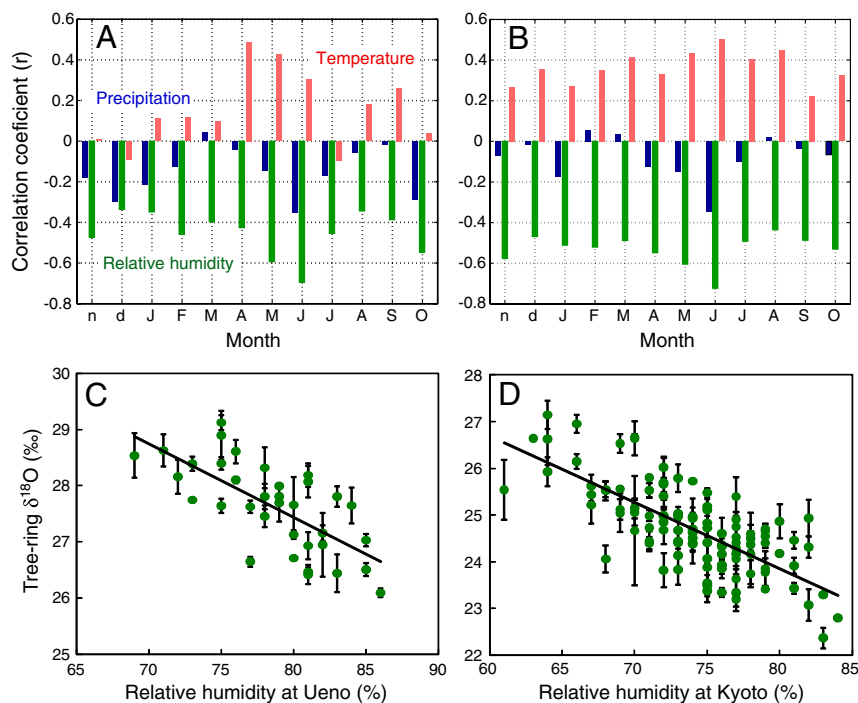


Fig. 1. Correlations between tree-ring cellulose $\delta^{18}\text{O}$ and meteorological data. (*A, B*) Correlation coefficients of the monthly temperature (red), precipitation (blue), and relative humidity (green) with the tree-ring cellulose $\delta^{18}\text{O}$ of the Nara cedar during A.D. 1938–1998 (*A*) and that of the Shiga cypress during A.D. 1881–1993 (*B*), respectively. Correlation coefficients were calculated for $\delta^{18}\text{O}$ relative to the monthly average of the climate data from the closest meteorological stations (Ueno and Kyoto, respectively) in the current year (capital letters) and the previous year (lower case letters). (*C, D*) Relationships between the relative humidity (RH) in June and the tree-ring cellulose $\delta^{18}\text{O}$ of the Nara cedar (*C*), that of the Shiga cypress (*D*). These can be expressed as follows: (*C*) $\delta^{18}\text{O} = (-0.1312 \pm 0.0236) \times \text{RH} + (37.93 \pm 1.857)$, $r = -0.695$, $p = 3.54 \times 10^{-6}$, $n = 35$. (*D*) $\delta^{18}\text{O} = (-0.1419 \pm 0.0129) \times \text{RH} + (35.20 \pm 0.955)$, $r = -0.723$, $p = 1.482 \times 10^{-19}$, $n = 113$. Error bars show the standard deviations ($\pm 1\sigma$) of replicate analysis of the tree-ring $\delta^{18}\text{O}$.

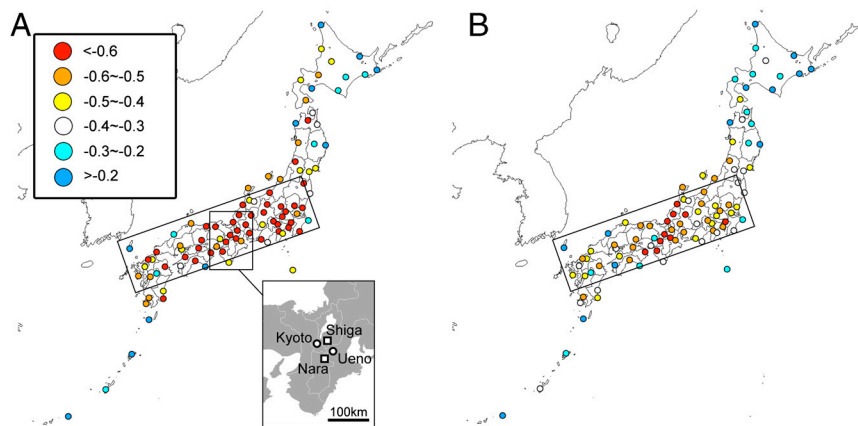


Fig. 2. (A) Correlation coefficients between the $\delta^{18}\text{O}$ of the Nara cedar and relative humidity in June from 96 meteorological stations across Japan during A.D. 1938–1998 ($n = 35$). Open squares in the right-bottom map indicate the sampling sites (Nara and Shiga) and open circles indicate the closest meteorological stations (Ueno and Kyoto, respectively). (B) Correlation coefficients between the $\delta^{18}\text{O}$ of the Shiga cypress and relative humidity in June from 96 meteorological stations across Japan during A.D. 1938–1993 ($n = 56$).

heliospheric current sheet (39, 40). As the dipole field reverses every 11 years at solar activity maxima, it results in the 22 year cycle in GCR flux, which is not apparent in solar irradiative outputs. Moreover, it has been suggested that the modulation of GCRs in the heliosphere depends on the level of solar activity, resulting in the different pattern in GCR variations between the present period and the grand solar minima (28, 29). During the “normal” state, as was in the past decades, the flux of GCRs is relatively high when the solar polarity is positive because the GCRs are less sensitive to the intensity of solar magnetic field during this time. However, the relationship between the relative intensity of GCRs and the solar polarity is inverted during prolonged inactive periods of the sun such as the Maunder Minimum. The GCR flux is likely to be high when the solar polarity is negative at this mode, because of the possibly of a flatter current sheet gathering GCRs from the horizontal direction (28, 29). The concordance between the three climate records and the pattern of GCR flux suggests that decadal-scale variations in solar activity and in GCR flux could be related to climate changes over the whole of the NH during and just after the Maunder Minimum. Moreover, the internally caused solar-like periodicities in climate variability can be excluded as the driver of these climate changes, because the lengths of solar cycles during this period are very characteristic and are different from those during the normal periods.

We also found negative $\delta^{18}\text{O}$ spikes in tree-ring cellulose from Japan that are weaker and broader than the spikes described above. They occur at solar minima with positive solar polarity during the Maunder Minimum (red dotted lines) and at solar minima with negative solar polarity after the Maunder Minimum (blue dotted line), when the GCR flux was lower than at the other solar minima. They can also be seen in Greenland temperature variations, although the intensity of some spikes is smaller than those found in Japan. They are not as clear in NH mean temperature records during the Maunder Minimum, whereas the signals were clearly detected at solar minima with high GCR intensity. This spatial pattern possibly suggests that the climate signals were too weak compared to the internally caused variations to affect the mean climate state of the NH at solar minima with low incident GCR intensity.

For extraction of these climate signals and reduction of noise in the records, superimposed variation of the tree-ring $\delta^{18}\text{O}$ and the ^{14}C production anomaly are shown in Fig. 4 over four solar magnetic cycles during the Maunder Minimum mode of solar cycles (see *Materials and Methods*). The influence of solar magnetic cycles can clearly be identified in $\delta^{18}\text{O}$ variations over Japan. Moreover, significant differences in the height and shape

of the peaks can be identified among the major spikes of each polarity. Major steep spike in $\delta^{18}\text{O}$ can be detected with a high level of significance (4 times larger than the standard deviation of the superposition data) only when the solar polarity is negative. We note that timing of the $\delta^{18}\text{O}$ peak is coincident with that of ^{14}C , suggesting that the climate in Japan responds rapidly to variations in solar activity and GCRs. Feedback mechanisms through ocean currents are excluded as these would require longer, decadal, lags in response times (23).

We hypothesize that annual-scale decrements in the $\delta^{18}\text{O}$ have been caused by steep GCRs changes at the solar minima of negative polarity. Numerical calculations of the propagation of GCRs in the heliosphere (40) suggests that the GCR flux could be substantially enhanced if the tilt angle of heliospheric current sheet reaches close to ~ 0 degrees, but only at times when the solar magnetic polarity is negative (Fig. S2). Normally the tilt angle does not approach to ~ 0 even at the minima of the solar cycle, but this may happen when solar activity is extremely low such as during the Maunder Minimum. The possibility of annual-scale enhancements of GCR flux at solar minima of negative polarity is supported by a ^{10}Be record from the NGRIP ice core in Greenland (38). The record shows quasi-periodic steep peaks of ^{10}Be flux around the Maunder Minimum (open circles in Fig. 3E). There is some uncertainty in dating of ice cores, however, the timing of the steep peaks in ^{10}Be flux (around A.D. 1640, 1670, 1700, and 1725) are generally consistent with the timing of solar minima of negative polarity deduced from the ^{14}C production anomaly and the steep negative spikes in our tree-ring $\delta^{18}\text{O}$ record (see the next paragraph). The difference of ^{10}Be flux between solar polarities should be originated from drift effect as described above, although the actual overall enhancement of GCR flux could be slightly smaller than the reconstruction by ^{10}Be records due to the possible local climate influence on ^{10}Be deposit (41). The signal of superimposed $\delta^{18}\text{O}$ around the solar minima of positive polarity is less significant and shows different shape, which could be explained by a broad signal of GCR flux (Fig. S2) and its relatively small amplitude comparable to the internally caused climate changes. The enhancement of the variability of GCR flux around the Maunder Minimum could also explain the reason why the signals of solar activity and GCRs are evident in the climate records only during this period. The variability of GCR flux has been relatively small during the normal periods; hence the influence of GCRs could be less significant and be buried within other climate variations. To confirm the hypothesized annual-scale enhancement of GCR flux at the solar minima of negative polarity, it will be important to refine and extend the annual-scale reconstructions of GCR flux using cos-

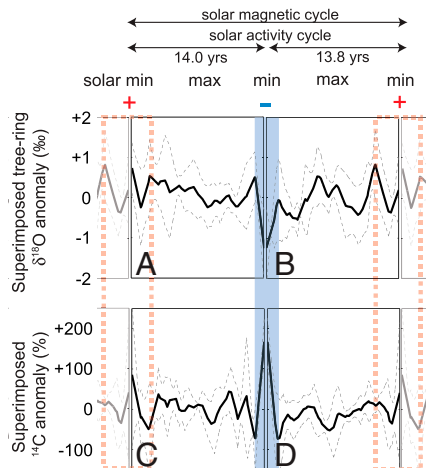


Fig. 4. Superimposition of the tree-ring $\delta^{18}\text{O}$ record and the ^{14}C production anomaly based on solar magnetic cycles during the Maunder Minimum mode of solar cycles. The filtered tree-ring $\delta^{18}\text{O}$ was superimposed for 4 solar activity cycles from the solar minima (GCR flux maxima) of positive polarity to that of negative polarity (A), and from that of negative polarity to that of positive polarity (B). The ^{14}C production anomaly was superimposed for the same period (C–D). Mean lengths of the 4 solar activity cycles for each polarity are shown below the arrows (14.0 years for A and C; 13.8 years for B and D). Standard deviations of the presuperimposed $\delta^{18}\text{O}$ and ^{14}C data during the 4 periods are shown as gray dotted line ($\pm 1\sigma$) in each panel. The left parts of (A, C) and the right parts of (B, D) are also shown with light colors in the right side of (B, D) and the left side of (A, C), respectively, for making it easy to see the solar signals in the solar minima of positive polarity. There is a large and steep negative spike at solar minimum of polarity negative (blue shaded; high GCR flux), and a relatively small and broad negative spike at solar minima of polarity positive (red dotted line; low GCR flux).

seasons in Japan, because they correlate negatively. For example, the relative humidity in June correlated negatively with the temperature in June during A.D. 1938–1998 in the closest meteorological station (Ueno) near the Nara cedar site ($r = -0.446$, $p < 0.001$). Moreover, the effects of solar activity and high GCR flux could persist throughout the year at solar minima because of the coincidence between high relative humidity in rainy seasons (June) in Japan, winter temperatures in Greenland and the mean annual temperatures in the NH.

We conclude that the variation of GCR flux associated with the multidecadal cycles of solar magnetic field could cause the significant and widespread Northern-Hemisphere scale climate changes at least during the Maunder Minimum. Similar studies of climate variability, targeting the Maunder Minimum and other anomalous solar periods such as the Spörer Minimum (A.D. 1416–1534), at higher spatial resolution including Southern Hemisphere with annual resolution are needed to confirm the global significance. Coupling $\delta^{18}\text{O}$ directly with $\Delta^{14}\text{C}$ derived from tree rings is likely to be a powerful tool to study the connections between the sun and climate change.

Materials and Methods

Sample Site and Materials. We used a disk of 392 year old (A.D. 1607–1998) Japanese cedar (*Cryptomeria japonica*) obtained from the Murou Temple in Nara, central Japan [34.32°N, 136.02°E, 405 m above sea level (a.s.l.)] and a disk of Japanese cypress (*Chamaecyparis obtuse*) obtained from Shiga, central Japan (34.55°N, 135.59°E, 550 m a.s.l.). $\Delta^{14}\text{C}$ in the Nara cedar tree rings was reported previously (27). Each ring from the Nara cedar was absolutely dated by detecting the peak of $\Delta^{14}\text{C}$ in 1964, which resulted from the nuclear bomb tests in the atmosphere (the “Bomb effect”), and by dendrodating, which is a pattern matching of the time sequence of tree-ring widths to that of the standard pattern (27). Tree rings of the Shiga cypress were also absolutely dated by dendrodating. For the calibration of the tree-ring cellulose $\delta^{18}\text{O}$ of the Nara cedar, monthly meteorological data, including temperature, precipitation, and relative humidity, were used. The records were available at the nearest meteorological station (Ueno meteorological station; 34.45°N,

136.08°E, 159 m a.s.l.) and covered the period A.D. 1938–1998. During this period, the maximum and minimum monthly mean temperatures were approximately 25.6 °C in August and 2.5 °C in January, respectively. The mean annual precipitation was 1440 mm. The monthly mean precipitation was maximum in June (213.7 mm). The monthly mean relative humidity was maximum in September (81.4%) and minimum in March (72.1%). For the Shiga cypress, data obtained at Kyoto meteorological station (35.01°N, 135.44°E, 41 m a.s.l.) during A.D. 1881–1993 were used. During this period, the maximum and minimum monthly mean temperatures were approximately 26.8 °C in August and 3.2 °C in January, respectively. The mean annual precipitation was 1577 mm. The monthly mean precipitation was maximum in June (238.1 mm). The monthly mean relative humidity was maximum in November (76.8%) and minimum in April (69.0%).

Sample Preparation. For the Nara cedar, individual growth rings were cut every year from A.D. 1612–1756 by using a razor blade. Each ring was sliced into 20 μm thick sections along the fibrous direction using a rotary microtome. Tree rings corresponding to 35 discontinuous years during A.D. 1938–1998 (1938–1942, 1946, 1948–1953, 1956–1958, 1979–1998) were directly sliced into 20 μm thick sections by the rotary microtome, because the ring widths during this period were too narrow to be cut by a razor blade. In the Shiga cypress, the individual yearly growth rings from A.D. 1973–1998 were cut by a razor blade and sliced into 20- μm -thick sections along the fibrous direction using the microtome. Tree rings from A.D. 1881–1972 were directly sliced into 20 μm thick sections similarly. α -cellulose was extracted from these sections (43).

$\delta^{18}\text{O}$ Measurement. The extracted α -cellulose was analyzed for $\delta^{18}\text{O}$ in duplicate by using a continuous flow system of a pyrolysis-type elemental analyzer (Thermo Quest TCEA) and an isotope ratio mass spectrometer (Thermo Quest Delta plus XL) (44). In the pyrolysis furnace packed with glassy carbon, oxygen in the cellulose was quickly converted to CO gas at 1375 °C. The standard deviation for repeated analysis of standard material was less than 0.2‰. The isotope ratio is expressed in the delta notation; i.e., $\delta^{18}\text{O} = ((^{18}\text{O}/^{16}\text{O})_{\text{sample}} / (^{18}\text{O}/^{16}\text{O})_{\text{standard}} - 1) \times 1000(\text{‰})$, relative to the international standard (Vienna Standard Mean Ocean Water) for oxygen.

Solar Cycles. The timings of solar cycle minima during the Maunder Minimum were obtained by calculating the effect of lag and attenuation between solar activity and $\Delta^{14}\text{C}$ records via the carbon cycle. The annual $\Delta^{14}\text{C}$ variation in tree rings (INTCAL1998) (25) was filtered with a bandwidth of 2–35 years to remove low-frequency component, and then ^{14}C production rate was calculated by the method described in (45). The errors of ^{14}C production anomaly was calculated from the analytical errors ($\pm 1\sigma$) of $\Delta^{14}\text{C}$ in (25) with lag and attenuation of 2 year frequency component. The lags between the high ^{14}C production anomaly and the solar sunspot minima may be due to the lags between variations of GCR flux and sunspots (46). The measurement errors of INTCAL are smaller than our $\Delta^{14}\text{C}$ errors in the Nara cedar (27); however, the short-term variations in the two $\Delta^{14}\text{C}$ records are consistent with each other (47).

Superimposition. The tree-ring $\delta^{18}\text{O}$ record and the calculated ^{14}C production anomaly were superimposed for 4 solar activity cycles from the solar minima (GCR flux maxima) of positive polarity to that of negative polarity (A.D. 1632–1640, 1657–1672, 1685–1700, 1711–1725; Fig. 4 A and C, respectively) and from that of negative polarity to that of positive polarity (A.D. 1640–1657, 1672–1685, 1700–1711, 1725–1735; Fig. 4 B and D, respectively) around the Maunder Minimum mode of solar cycles. The $\delta^{18}\text{O}$ record was filtered with a bandpass of 2–35 years to remove low-frequency component before superimposition. The solar minima were determined as the high peaks of ^{14}C production anomaly during and just before the Maunder Minimum mode (A.D. 1632–1725). The solar minimum just after the Maunder Minimum mode (A.D. 1735) was determined from the sunspot minimum, because it was difficult to determine from the ^{14}C production anomaly. The lag between variation of sunspots and GCR flux (46) was corrected by adding 1 year from the sunspots minimum (A.D. 1734).

ACKNOWLEDGMENTS. We thank K. Ohnishi for helping with the analysis of tree-ring cellulose $\delta^{18}\text{O}$, K. Masuda for providing the Nara cedar tree, K. Nagaya and K. Kitazawa for their help in sampling the cedar tree sticks, A.-M. Berggren and J. Beer for providing the NGRIP ^{10}Be data, and T.M. Esat for comments. We also thank two anonymous reviewers and the editor for helpful and constructive criticisms during the review process. This work has been partly supported by a grant from the Japan Society for the Promotion of Science (Y.Y., T.N., and H.M.) and Global Environmental Research Fund (Y.Y.).

1. Bard E, Frank M (2006) Climate change and solar variability: What's new under the sun? *Earth Planet Sc Lett* 248:1–14.
2. Foukal P, North G, Wigley T (2004) A stellar view on solar variations and climate. *Science* 306:68–69.
3. Foukal P, Fröhlich C, Spruit H, Wigley TML (2006) Variations in solar luminosity and their effect on the Earth's climate. *Nature* 443:161–166.
4. Lean J (2000) Evolution of the sun's spectral irradiance since the Maunder Minimum. *Geophys Res Lett* 27:2425–2428.
5. Hood LL (1986) Stratospheric ozone and temperature responses to short-term changes in solar ultraviolet flux: An analysis of Nimbus 7 SBUV and SAMS data. *J Geophys Res* 91:5264–5276.
6. Lean J, White OR, Skumanich A (1995) On the solar ultraviolet spectral irradiance during the Maunder Minimum. *Global Biogeochem Cy* 9:171–182.
7. Hood LL, Soukharev B (2003) Quasi-decadal variability of the tropical lower stratosphere: The role of extra tropical wave forcing. *J Atmos Sci* 60:2389–2403.
8. Meehl GA, Arblaster JM, Matthes K, Sassi F, van Loon H (2009) Amplifying the Pacific climate system response to a small 11-year solar cycle forcing. *Science* 325:1114–1118.
9. Svensmark H, Friis-Christensen E (1997) Variation of cosmic ray flux and global cloud coverage—A missing link in solar–climate relationships. *J Atmos Sol-Terr Phys* 59:1225–1232.
10. Marsh ND, Svensmark H (2000) Low cloud properties influenced by cosmic rays. *Phys Rev Lett* 85:5004–5007.
11. Carslaw KS, Harrison RG, Kirkby J (2002) Cosmic rays, clouds, and climate. *Science* 298:1732–1737.
12. Svensmark H (2007) Cosmoclimatology: A new theory emerges. *Astron Geophys* 48:1.18–1.24.
13. Svensmark H, Bondo T, Svensmark J (2009) Cosmic ray decreases affect atmospheric aerosols and clouds. *Geophys Res Lett* 36:L15101.
14. Bond G, et al. (2001) Persistent solar influence on north Atlantic climate during the Holocene. *Science* 294:2130–2136.
15. Hodeell DA, Brenner M, Curtis JH, Guilderson T (2001) Solar forcing of drought frequency in the Maya lowlands. *Science* 292:1367–1370.
16. Hu FS, et al. (2003) Cyclic variation and solar forcing of holocene climate in the Alaskan subarctic. *Science* 301:1890–1893.
17. Polissar PJ, et al. (2006) Solar modulation of Little Ice Age climate in the tropical Andes. *Proc Natl Acad Sci USA* 103:8937–8942.
18. Neff U, et al. (2001) Strong coherence between solar variability and the monsoon in Oman between 9 and 6 kyr ago. *Nature* 411:290–293.
19. Fleitmann D, et al. (2003) Holocene forcing of the Indian monsoon recorded in a stalagmite from Southern Oman. *Science* 300:1737–1739.
20. Wang Y, et al. (2005) The Holocene Asian monsoon: links to solar changes and North Atlantic climate. *Science* 308:854–857.
21. Zhang P, et al. (2008) A test of climate, sun, and culture relationships from an 1810 year Chinese cave record. *Science* 322:940–942.
22. Dunbar RB, Wellington GM, Colgan MW, Glynn PW (1994) Eastern Pacific sea surface temperature since 1600 A. D.: The $\delta^{18}\text{O}$ record of climate variability in Galapagos corals. *Paleoceanography* 9:291–315.
23. Eichler A, et al. (2009) Temperature response in the Altai region lags solar forcing. *Geophys Res Lett* 36:L01808.
24. Pederson N, Jacoby GC, D'Arrigo RD, Cook ER, Buckley BM (2001) Hydrometeorological reconstructions for northeastern Mongolia derived from tree rings: 1651–1995. *J Climate* 14:872–881.
25. Stuiver M, Reimer PJ, Braziunas TF (1998) High-precision radiocarbon age calibration for terrestrial and marine samples. *Radiocarbon* 40:1127–1151.
26. Eddy JA (1976) The Maunder Minimum. *Science* 192:1189–1202.
27. Miyahara H, et al. (2004) Cyclicity of solar activity during the Maunder Minimum deduced from radiocarbon content. *Sol Phys* 224:317–322.
28. Jokipii JR (1991) Variations of the cosmic-ray flux with time. *The Sun in Time*, eds CP Sonnett et al. (University of Arizona Press, Tucson), pp 205–220.
29. Miyahara H, Yokoyama Y, Masuda K (2008) Multi-decadal climate cycles controlled by the periodic reversals of solar magnetic field polarity. *Earth Planet Sc Lett* 272:290–295.
30. Vinther BM, Johnsen SJ, Andersen KK, Clausen HB, Hansen AW (2003) NAO signal recorded in the stable isotopes of Greenland ice cores. *Geophys Res Lett* 30:1387–1390.
31. McCarroll D, Loader NJ (2004) Stable isotopes in tree rings. *Quaternary Sci Rev* 23:771–801.
32. Araguas-Araguas L, Fröhlich K, Rozanski K (1998) Stable isotope composition of precipitation over southeast Asia. *J Geophys Res* 103:28721–28742.
33. Nakatsuka T, et al. (2004) Oxygen and carbon isotopic ratios of tree-ring cellulose in a conifer-hardwood mixed forest in northern Japan. *Geochemical J* 38:77–88.
34. Tsuji H, Nakatsuka T, Takagi K (2006) $\delta^{18}\text{O}$ of tree-ring cellulose in two species (spruce and oak) as proxies of precipitation amount and relative humidity in northern Japan. *Chem Geol* 231:67–76.
35. Tsuji H, Nakatsuka T, Yamazaki K, Takagi K (2008) Summer relative humidity in northern Japan inferred from $\delta^{18}\text{O}$ values of the tree ring in (1776–2002 A.D.): Influence of the paleoclimate indices of atmospheric circulation. *J Geophys Res* 113:D18103.
36. Mann ME, Bradley RS, Hughes MK (1999) Northern Hemisphere temperatures during the past millennium: Inferences, uncertainties, and limitations. *Geophys Res Lett* 26:759–762.
37. Hoyt DV, Schatten KH (1998) Group sunspot numbers: A new solar activity reconstruction. *Sol Phys* 179:189–219.
38. Berggren AM, et al. (2009) A 600-year annual ^{10}Be record from the NGRIP ice core, Greenland. *Geophys Res Lett* 36:L11801.
39. Kota J, Jokipii JR (1983) Effect of drift on the transport of cosmic rays. VI. A three-dimensional mode including diffusion. *Astrophys J* 265:573–581.
40. Kota J, Jokipii JR (2001) 3-D modeling of cosmic-ray transport in the heliosphere: Toward solar maximum. *Adv Space Res* 27:529–534.
41. Webber WR, Higbie PR (2010) What Voyager cosmic ray data in the outer heliosphere tells us about ^{10}Be production in the Earth's polar atmosphere in the recent past. *J Geophys Res* 115:A05102.
42. Usoskin IG, Marsh N, Kovaltsov GA, Mursula K, Gladysheva OG (2004) Latitudinal dependence of low cloud amount on cosmic ray induced ionization. *Geophys Res Lett* 31:L16109.
43. Loader NJ, Robertson I, McCarroll D (2003) Comparison of stable carbon isotope ratios in the whole wood, cellulose and lignin of oak tree-rings. *Palaeogeogr Palaeoclimatol Palaeoecol* 196:395–407.
44. Sharp ZD, Atudorei V, Durakiewicz T (2001) A rapid method for determination of hydrogen and oxygen isotope ratios from water and hydrous minerals. *Chem Geol* 178:197–210.
45. Siegenthaler U, Beer J (1988) Model comparison of ^{14}C and ^{10}Be isotope records. *Secular Solar and Geomagnetic Variations in the Last 10,000 Years*, eds FR Stephenson and AW Wolfendale (Kluwer, Boston), pp 315–328.
46. Cliver EW, Ling AG (2001) 22 year patterns in the relationship of sunspot number and tilt angle to cosmic-ray intensity. *Astrophys J Lett* 551:L189–L192.
47. Miyahara H, et al. (2007) Variation of solar activity from the Spoerer to the Maunder minima indicated by radiocarbon content in tree-rings. *Adv Space Res* 40:1060–1063.